

Two-Fluid Marangoni–Bénard Convection with a Deformable Interface

S. J. Tavener* and K. A. Cliffe†

**Department of Mathematics, Colorado State University, Fort Collins, Colorado 80523;*
and †*Serco Assurance, Harwell, United Kingdom*

E-mail: tavener@math.colostate.edu and andrew.cliffe@sercoassurance.com

Received June 26, 2001; revised June 28, 2002

Two immiscible fluid layers that are subjected to a temperature gradient perpendicular to their interface exhibit a range of behaviors that is considerably richer than for the single-fluid case. We describe a numerical technique for calculating thermally driven flows in two fluid layers which uses a simple technique based on a Landau transformation to map the physical domain into a reference domain, enabling the unknown location of the deformable interface to be determined. The coupled system of nonlinear partial differential equations, comprising mapping, continuity, momentum, and energy equations and the appropriate boundary conditions, is solved using the finite-element method in two-dimensional domains. Numerical bifurcation techniques are used to investigate the multiplicity of the solution set. The case of heating from above is considered in some detail and the results of finite-element computations are compared with linear stability calculations performed on unbounded domains. The principal advantages of the finite-element approach are the ability to determine the effect of non-90° contact angles (when the conducting solution no longer exists and traditional linear stability approaches fail), the ability to determine the role of finite aspect ratio domains and the relative volume fractions of the two fluids, and the capability of calculating the nonlinear development of flows beyond the critical temperature gradient. © 2002 Elsevier Science (USA)

Key Words: two-fluid flow; Marangoni–Bénard convection; deformable interface.

1. INTRODUCTION

When a vertical temperature gradient is applied across a thin horizontal layer of a single fluid whose surface is exposed to the atmosphere, convective motion arises above a critical applied temperature difference. Convection may be driven either by bulk forces arising from temperature-induced density differences (buoyancy) or by surface forces due to the temperature-dependent nature of the surface tension (thermocapillarity). The relative size of

these two effects depends on the depth of the fluid layer, with thermocapillary forces dominating in sufficiently thin layers. Pioneering work on the relative importance of thermocapillarity and buoyancy for single fluids was performed by Block [1], Pearson [2], and Nield [3].

The range of possible behaviors when two immiscible fluid layers are confined between parallel plates and subjected to a temperature gradient perpendicular to the plates is considerably richer. For example, the layers may be unstable when heated from above, despite the fact that their density increases in the same direction as the gravity vector and thus the fluids are stably stratified. The motions in the two layers may be thermally coupled rather than viscously coupled. In this surprising flow regime, clockwise convective motions in the upper layer lie on top of clockwise rolls in the lower layer (and similarly for anticlockwise rolls). Unlike the single fluid case, time-dependent flows may develop directly from the conducting solution. A comprehensive review of the considerable literature to date is provided by Velarde *et al.* [4] and by Andereck *et al.* [5].

The preponderance of stability analyses have been performed assuming unbounded or periodic domains. For example, Zeren and Reynolds [6] predicted the onset of convection on heating from above but were unable to find it experimentally. Imaishi and Fujinawa [7, 8] extended the stability analysis of Nield [3] (including both gravitational and surface tension effects) to two-fluid systems but assumed an undeformable interface and did not consider time-dependent disturbances. Rasanat *et al.* [9] considered layers of almost equal densities and predicted the onset of oscillatory instabilities but were unable to detect them experimentally. Their analysis was extended considerably by Renardy and Joseph [10] and Renardy and Renardy [11, 12]. Recently Juel *et al.* [13] observed experimentally both the onset of convection on heating from above and oscillatory motion at onset in two-fluid systems.

Surprisingly few two- or three-dimensional computations have been reported in the literature. Géoris *et al.* [14, 15] performed finite-difference computations with a nondeforming interface in a three-layer system and compared their results with experiment. Recently, Johnson and Narayanan [16, 17] recognized the need for stability calculations to be performed in bounded domains, due to the number of experiments performed in small-aspect ratio devices (e.g., [5, 18]) and because of the necessarily finite domains in industrial applications. Much of the recent interest in two-fluid systems has been motivated by the liquid encapsulated vertical Bridgman (LEVB) process, used, for example, to grow crystals of gallium arsenide. Thermocapillary instabilities arising in the melt can affect the quality of the resulting crystal and the distribution of dopants and can limit the operating conditions under which crystals are grown. During the manufacturing process the relative volume fractions of the two fluids and the aspect ratios of the two-fluid domains vary, profoundly affecting the stability of the system. The numerical techniques we have developed and which are described here have been designed to cope with both such changes in an efficient manner.

In this paper we compute the two-fluid Rayleigh–Marangoni–Bénard convection problem in finite rectangular domains with a deformable interface between the two fluids. Nonlinearities are present both in the governing equations which pertain within each fluid and in the boundary conditions at the deformable interface between the two fluids. A jump in pressure exists across the interface that is proportional to the product of the curvature of the interface and the (temperature dependent) interfacial tension. We solve the full nonlinear problem and make no assumptions regarding the relative sizes of the inertial and diffusive terms in the momentum equations, or the relative magnitudes of the properties of the two fluids. The contact angle is not required to be close to 90 degrees, nor is the free surface curvature required to be small.

Cliffe and Tavener [19] used the finite-element method, coupled with numerical bifurcation techniques, to determine the quantitative effect of free-surface deformations on the bifurcation structure in two-dimensional single-fluid Marangoni–Bénard convection systems. For contact angles other than 90 degrees, the free surface is no longer an isothermal surface, and shear stresses exist along the free surface, arising from the temperature-dependent nature of the surface tension. There is no conducting solution that satisfies both the equilibrium and boundary conditions, and flows comprising an even numbers of cells develop continuously as the applied temperature gradient is increased. An analogous phenomena is observed in multiple fluid layers when the contact angle between the fluid interface and the vertical domain walls is other than 90 degrees.

We do not attempt in this paper to locate the onset of oscillatory flows. To do so efficiently would require a robust strategy for solving the generalized eigenvalue problem that results from a linear stability analysis and, in particular, for determining those generalized eigenvalues with the smallest real part. An efficient numerical technique for finding these “most dangerous eigenvalues” when a mixed finite-element method is used to discretize the Navier–Stokes equations has been developed by Cliffe *et al.* [20] and has been applied, for example, to determine the linear stability of flow past a sphere in a pipe [21]. This technique makes extensive use of the special block structure of the generalized eigenvalue problem. Efficient ways to utilize the more complicated block structure that arises when two different fluids are coupled via a deformable interface are currently under investigation. While it would be possible to construct an extended system to locate Hopf bifurcation points (see, e.g., [22]), without a good estimate for the critical parameter values and eigenvector, discovery of a Hopf bifurcation point in this manner would be merely serendipitous. We concentrate instead on regions of parameter space in which steady behavior is expected according to the work of Juel *et al.* [13].

2. GOVERNING EQUATIONS

Consider the flow in the two-dimensional domain sketched in Fig. 1. Applying the Boussinesq approximation and using $*$ to denote dimensional quantities and derivatives with respect to dimensional quantities, the system of equations governing two-fluid Rayleigh–Marangoni–Bénard convection in finite two-dimensional domains with velocity \mathbf{u}^* , pressure p^* , and temperature T^* is

$$\nabla_* \cdot \mathbf{u}^* = 0, \quad (1)$$

$$\bar{\rho}_m \left(\frac{\partial \mathbf{u}^*}{\partial t^*} + (\mathbf{u}^* \cdot \nabla_*) \mathbf{u}^* \right) = \nabla_* \cdot \boldsymbol{\tau}_m^* - \rho_m g \mathbf{j}, \quad (2)$$

$$\bar{\rho}_m c_m \left(\frac{\partial T^*}{\partial t^*} + (\mathbf{u}^* \cdot \nabla_*) T^* \right) = \nabla_* \cdot (k_m \nabla_* T^*). \quad (3)$$

Here $\rho_m = \bar{\rho}_m (1 - \alpha_m (T^* - \bar{T}^*))$ is the density of liquid m , \bar{T}^* is a fixed reference temperature, c_m is the specific heat capacity, k_m is the thermal conductivity,

$$\boldsymbol{\tau}_m^* = -p^* \mathbf{I} + \mu_m (\nabla_* \mathbf{u}^* + (\nabla_* \mathbf{u}^*)^T)$$

is the stress tensor, and μ_m is the molecular diffusivity. The subscript $m = 1, 2$ denotes the

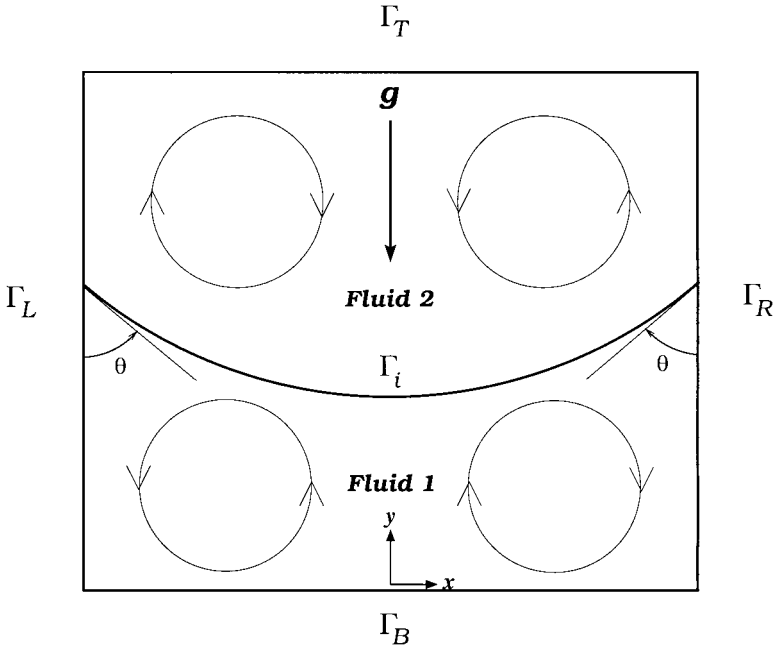


FIG. 1. Sketch of the physical domain.

lower and upper fluids, respectively. Here

$$\nabla_* = \mathbf{i} \frac{\partial}{\partial x^*} + \mathbf{j} \frac{\partial}{\partial y^*}, \quad \nabla_*^2 = \frac{\partial^2}{\partial x^{*2}} + \frac{\partial^2}{\partial y^{*2}},$$

where \mathbf{i} and \mathbf{j} are unit vectors in the x - and y -directions, respectively. The boundary conditions at the interface are

$$\mathbf{u}^* \cdot \mathbf{n} = 0, \quad (4)$$

$$[\boldsymbol{\tau}^* \cdot \mathbf{n}] = \boldsymbol{\tau}_2^* \cdot \mathbf{n} - \boldsymbol{\tau}_1^* \cdot \mathbf{n} = -K^* \sigma \mathbf{n} - (\mathbf{t} \cdot \nabla_* \sigma) \mathbf{t}, \quad (5)$$

$$[k(\nabla_* T^* \cdot \mathbf{n})] = k_2(\nabla_* T^* \cdot \mathbf{n})_2 - k_1(\nabla_* T^* \cdot \mathbf{n})_1 = 0, \quad (6)$$

where K^* is the (dimensional) curvature of the interface, $[\cdot]$ denotes the jump across the interface, and \mathbf{n} and \mathbf{t} are the normal and tangential unit vectors, respectively. By convention, \mathbf{n} is the normal vector directed from fluid 1 into fluid 2. The interfacial tension is assumed to depend linearly on the temperature, and $\sigma = \sigma_0 - \sigma_1(T^* - \bar{T}^*)$.

We nondimensionalized Eqs. (1)–(3) and boundary conditions (4)–(6) using the distance between the plates $d = d_1 + d_2$ as the length scale. This choice was based on our desire to perform continuation with respect to the volume fraction. Choosing d_1 as the length scale would mean that in such continuation studies all nondimensional groups involving the length scale would change simultaneously, a situation we wished to avoid. The velocity scale was chosen to be κ_1/d , where κ_1 is the thermal diffusivity of the lower fluid, and $\kappa_1 = k_1/(\bar{\rho}_1 c_1)$. The corresponding time and stress scales were d^2/κ_1 and $\mu_1 \kappa_1/d^2$, respectively. The temperature was nondimensionalized as $T = (T^* - \bar{T}^*)/\Delta T^*$, where ΔT^* is one-half the temperature difference between the top and bottom boundaries. This choice of

the temperature scale was made in order to simplify initial comparisons with known results for a single fluid. (Marangoni and Rayleigh numbers based on a temperature scale equal to the difference in temperature between the two plates can be obtained by multiplying the values reported here by a factor of two.)

The nondimensionalized weak form of the steady equations corresponding to the above choices is

$$\int_{\Omega_1} (\nabla \cdot \mathbf{u})q \, dA + \int_{\Omega_2} (\nabla \cdot \mathbf{u})q \, dA = 0, \quad (7)$$

$$\begin{aligned} & \int_{\Omega_1} \left[\left(\frac{1}{Pr} (\mathbf{u} \cdot \nabla) \mathbf{u} + (G - Ra T) \mathbf{j} \right) \cdot \mathbf{w} - p \nabla \cdot \mathbf{w} + (\nabla \mathbf{u} + \nabla \mathbf{u}^T) : \nabla \mathbf{w} \right] dA \\ & + \int_{\Omega_2} \left[\rho_r \left(\frac{1}{Pr} (\mathbf{u} \cdot \nabla) \mathbf{u} + (G - \alpha_r Ra T) \mathbf{j} \right) \cdot \mathbf{w} - p \nabla \cdot \mathbf{w} + \mu_r (\nabla \mathbf{u} + \nabla \mathbf{u}^T) : \nabla \mathbf{w} \right] dA \\ & + \int_{\Gamma_i} \left(\frac{1}{Ca} - Ma T \right) \mathbf{t} \cdot \frac{d\mathbf{w}}{ds} \, ds = 0, \end{aligned} \quad (8)$$

$$\int_{\Omega_1} ((\mathbf{u} \cdot \nabla T) \xi + \nabla T \cdot \nabla \xi) \, dA + \int_{\Omega_2} (\rho_r c_r (\mathbf{u} \cdot \nabla T) \xi + k_r \nabla T \cdot \nabla \xi) \, dA = 0, \quad (9)$$

where Ω_1 , Ω_2 are the two-fluid regions, Γ_i is the interface between them, and q , \mathbf{w} , and ξ are test functions (see the Appendix for details.) The nondimensional parameters are the Prandtl number, Pr , the Galileo number, G , the capillary number, Ca , the Rayleigh number, Ra , and the Marangoni number, Ma , defined by

$$Pr = \frac{\nu_1}{\kappa_1}, \quad G = \frac{gd^3}{\nu_1 \kappa_1}, \quad Ca = \frac{\mu_1 \kappa_1}{\sigma_0 d}, \quad Ra = \frac{g \alpha_1 \nabla T^* d^3}{\nu_1 \kappa_1}, \quad Ma = \frac{\sigma_1 \nabla T^* d}{\mu_1 \kappa_1},$$

where $\nu_1 = \mu_1 / \bar{\rho}_1$. The ratios appearing in the integrals to be evaluated in Ω_2 , i.e., ρ_r , α_r , μ_r , c_r , and k_r , are

$$\rho_r = \frac{\bar{\rho}_2}{\bar{\rho}_1}, \quad \alpha_r = \frac{\alpha_2}{\alpha_1}, \quad \mu_r = \frac{\mu_2}{\mu_1}, \quad c_r = \frac{c_2}{c_1}, \quad \text{and} \quad k_r = \frac{k_2}{k_1}.$$

Finally, we defined the volume ratio to be

$$v_r = \frac{\text{volume fluid 2}}{\text{volume fluid 1}},$$

and the aspect ratio to be

$$\lambda = \frac{l}{d},$$

where l is the distance between the vertical side walls. To determine the unknown location of the interface, these equations were coupled to a Landau coordinate transformation,

$$\begin{aligned} x &= \lambda \psi, \quad y = 2h(\psi)\phi \quad \text{in fluid 1,} \\ x &= \lambda \psi, \quad y = 1 - 2(1 - h(\psi))(1 - \phi) \quad \text{in fluid 2.} \end{aligned}$$

The (unknown) height of the interface $h = h(\psi)$ was then calculated by coupling the differential equation

$$\frac{\partial h}{\partial \phi} = 0 \quad (10)$$

to Eqs. (1)–(3) and imposing the kinematic boundary condition (4). This was achieved by rewriting (10) in weak form,

$$\int_{\Omega_1} \frac{\partial h}{\partial \phi} \zeta \, dA + \int_{\Omega_2} \frac{\partial h}{\partial \phi} \zeta \, dA = 0, \quad (11)$$

with test function ζ and solving (11) simultaneously with Eqs. (7)–(9). Thus

$$\mathbf{u} = \mathbf{u}(x(\psi), y(h(\psi), \phi)), \quad p = p(x(\psi), y(h(\psi), \phi)), \quad T = T(x(\psi), y(h(\psi), \phi)),$$

where (ψ, ϕ) are the coordinates in the reference domain

$$\Omega_{\text{ref}} = \{(\psi, \phi) : (\psi, \phi) \in [-0.5, 0.5] \times [0, 1]\}.$$

Let

$$\Omega_{1,\text{ref}} = \{(\psi, \phi) : (\psi, \phi) \in [-0.5, 0.5] \times [0, 0.5]\},$$

$$\Omega_{2,\text{ref}} = \{(\psi, \phi) : (\psi, \phi) \in [-0.5, 0.5] \times [0.5, 1]\}.$$

All computations were performed in the reference domain Ω_{ref} . Nonslip boundary conditions were imposed at horizontal ($\phi = 0, 1$) and vertical ($\psi = \pm 0.5$) solid boundaries. The temperature was specified along the top and bottom surfaces and adiabatic conditions were applied at the vertical walls. Heating from above or from below was achieved by appropriate choice of the temperature boundary conditions at the top and bottom surfaces. The two contact angles were defined at $(\psi, \phi) = (\pm 0.5, 0.5)$ and the interfacial integral was evaluated along $\phi = 0.5$. The volume ratio was imposed by specifying the area A_1 of $\Omega_{1,\text{ref}}$. The area of Ω_2 was then given by $A_{2,\text{ref}} = 1 - A_{1,\text{ref}}$.

3. FINITE-ELEMENT SOLUTION TECHNIQUE

The weak equations (7)–(9) and (11) and the boundary conditions described above were solved using the finite-element method. All the computations reported below were performed using isoparametric quadrilateral elements with biquadratic interpolation of the height of the interface, h , the velocity components u and v , and the temperature, T . Discontinuous linear interpolation was employed for the pressure field. Noting that

$$\mathbf{u} \cdot \mathbf{n} = 0 \quad \text{on } \delta\Omega_{1,\text{ref}},$$

we recognize that one of the (local) element divergence constraints is redundant, and it is replaced by a constraint on the volume of fluid 1. Since the volumes of fluids 1 and 2 are not independent, this single constraint was sufficient to control the volume of fluid 2 as well. The pressure was normalized by specifying its value at one particular point. When extended

system techniques are used to locate bifurcation points, not only must the weak form itself be evaluated, but a number of its derivatives with respect to both variables and parameters are required. All subroutines to evaluate the weak form and its derivatives were written using a pre-processor, ENTICODE, based on Mathematica. A discussion of this technique appears in [23].

The nonlinear system of equations resulting from the finite-element discretization may be written as

$$\mathbf{f}(\mathbf{a}, \mathbf{b}) = 0, \quad \mathbf{f} : \mathbb{R}^N \times \mathbb{R}^p \mapsto \mathbb{R}^N. \quad (12)$$

Let S be a finite-dimensional representation of the reflectional symmetry operator about $\psi = 0$; thus S is an $(N \times N)$ orthogonal matrix, where $S^2 = I$ but $S \neq I$. The finite-dimensional system of nonlinear algebraic equations (12) is equivariant with respect to S ; i.e.,

$$S\mathbf{f}(\mathbf{a}, \mathbf{b}) = \mathbf{f}(S\mathbf{a}, \mathbf{b}). \quad (13)$$

The orthogonal matrix S induces a unique decomposition of \mathbb{R}^N into symmetric and anti-symmetric subspaces,

$$\mathbb{R}^N = \mathbb{R}_s^N \oplus \mathbb{R}_a^N,$$

where

$$\begin{aligned} \mathbb{R}_s^N &= \{\mathbf{x} \in \mathbb{R}^N : S\mathbf{a} = \mathbf{a}\}, \\ \mathbb{R}_a^N &= \{\mathbf{x} \in \mathbb{R}^N : S\mathbf{a} = -\mathbf{a}\}. \end{aligned}$$

Symmetric solutions are those for which

$$\begin{aligned} h(\psi, \phi) &= h(-\psi, \phi), \\ u(\psi, \phi) &= -u(-\psi, \phi), \\ v(\psi, \phi) &= v(-\psi, \phi), \\ p(\psi, \phi) &= p(-\psi, \phi), \\ T(\psi, \phi) &= T(-\psi, \phi). \end{aligned}$$

Antisymmetric solutions are those for which

$$\begin{aligned} h(\psi, \phi) &= -h(-\psi, \phi), \\ u(\psi, \phi) &= u(-\psi, \phi), \\ v(\psi, \phi) &= -v(-\psi, \phi), \\ p(\psi, \phi) &= -p(-\psi, \phi), \\ T(\psi, \phi) &= -T(-\psi, \phi). \end{aligned}$$

At a symmetry-breaking bifurcation point $(\mathbf{a}_0, \mathbf{b}_0)$,

$$\left. \frac{\partial \mathbf{f}}{\partial \mathbf{a}} \right|_{(\mathbf{a}_0, \mathbf{b}_0)} \mathbf{z} = 0,$$

where $\mathbf{a}_0 \in \mathbb{R}_s^N$ and the null eigenvector $\mathbf{z} \in \mathbb{R}_a^N$. Since the symmetries of the solution and eigenvector are known, all computations may be performed in one-half of the domain. Let Ω_{ref}^- be defined as

$$\Omega_{\text{ref}}^- = \left\{ (\psi, \phi) : (\psi, \phi) \in \left[-\frac{1}{2}, 0 \right] \times [0, 1] \right\}.$$

When computing a symmetric solution on Ω_{ref}^- , a global volume constraint is required. Nonslip velocity boundary conditions are imposed along $\phi = 0, 1$ and $\psi = -1/2$, and $u = 0$ along the symmetry axis $\psi = 0$ (by symmetry). The kinematic condition is applied along the interface $\phi = 0.5$. In other words

$$\mathbf{u} \cdot \mathbf{n} = 0 \quad \text{on } \delta\Omega_{1,\text{ref}}^-$$

(and similarly $\mathbf{u} \cdot \mathbf{n} = 0$ on $\delta\Omega_{2,\text{ref}}^-$). As before, it suffices to replace one of the (local) element divergence constraints with a volume constraint. However, when computing the null eigenvector on one-half of the domain, the u -velocity component of the eigenvector \hat{u} is not required to vanish by symmetry along $\psi = 0$ and all element divergence constraints are required. A volume constraint is therefore *not* applied to the eigenvector.

The linearized kinematic condition along the interface is

$$-u \frac{\partial \hat{h}}{\partial \psi} + \lambda v - \hat{u} \frac{\partial h}{\partial \psi} + \lambda \hat{v} = 0, \quad (14)$$

where h , u , and v are components of the solution, \hat{h} , \hat{u} , and \hat{v} are components of the perturbation, and λ is the aspect ratio. When using the Werner–Spence extended system [24] to locate symmetry-breaking points, Eq. (14) is used to determine the h -component of the null eigenvector \hat{h} at each node along the free surface. For all symmetric solutions, regardless of the value of the contact angle, the velocity components u and v are zero at the center of the free surface, since both $u = 0$ and $\partial h / \partial \psi = 0$ by symmetry. (The latter condition requires that the free surface has zero slope at the centerline and therefore $v = 0$ at the centerline.) At the symmetry axis, Eq. (14) reduces to

$$\hat{v} = 0. \quad (15)$$

For symmetric solutions, the v -component of velocity is symmetric about $\psi = 0$, so the v -component of a symmetry-breaking eigenvector must be antisymmetric about $\psi = 0$, and therefore \hat{v} must be zero along the symmetry axis. The kinematic condition (15) used to determine \hat{h} at the middle of the free surface is therefore identical to the condition on \hat{v} which is imposed by symmetry, and a naive implementation will have two linearly dependent equations. A nonsingular system of equations is obtained by replacing (15) at $\psi = 0$ with $\hat{h} = 0$, since the h -component of the eigenvector must be zero along $\psi = 0$ by reason of it being antisymmetric about $\psi = 0$. With these extra conditions, the Werner–Spence extended system [24] can be used as usual.

3.1. Subspace-Breaking Bifurcations

Two-cell (even cell) flows are symmetric with respect to the midplane symmetry and so do not develop as a result of breaking of the midplane symmetry. Rather, bifurcation to

even-cell flows is associated with the breaking of a subspace in which the velocity field is zero. (For a discussion of subspace breaking and methods for computing subspace-breaking bifurcations, see [25, 26].) An extended system similar to the Werner–Spence system is constructed, and by appropriate application of boundary conditions, the conducting solution is required to lie within a subspace in which the velocity field is identically zero, while the null eigenvector is required to lie outside this subspace (and have a nontrivial velocity field).

When computing the onset of two-cell (even cell) flows the null eigenvector is symmetric and the problems described in the previous section do not arise. There is no symmetry requirement for \hat{v} to be zero along the centerline. Indeed in the interior of the convecting flow, the v -component of the eigenvector is nonzero along $\psi = 0$ and is required to be zero at the free surface due to the kinematic boundary condition only. (For symmetric solutions, the free surface must be horizontal at the centerline and $u = 0$ along the centerline.) When computing bifurcations from symmetric flows to other symmetric flows on Ω_{ref}^- , the global constraint must be retained when computing the eigenvector, since for symmetric eigenvectors

$$\hat{\mathbf{u}} \cdot \mathbf{n} = 0 \quad \text{on } \delta\Omega_{1,\text{ref}}^-$$

4. RESULTS

4.1. Static Meniscus Problems

As a first test of the Landau transformation technique we computed the shape of the interface between two isothermal fluid layers with a fixed contact angle other than 90 degrees. In the absence of gravity the equilibrium-free surface is the arc of a circle. The L_2 difference between the computed and exact interface locations is reported in Table I. The jump in pressure across the free surface is the product of the (constant) curvature and the surface tension. The L_2 difference between the computed pressure in the lower fluid and the exact value is reported in Table II. Finally, the convergence of the velocity field (towards zero) is given in Table III. The observed quadratic convergence rate for both the pressure field and the interface location is something of a surprise, as linear convergence was observed by Cliffe and Tavener [19] using an orthogonal transformation. We suggest that the free surface location converges at one order lower than the velocity field, since the location of the free surface is essentially determined by the kinematic condition which involves derivatives of the velocity field. All calculations were performed with parameter values $Ra = 0$, $Ma = 10$, $Pr = 1$, $G = 0$, $Ca = 10^{-2}$, $\rho_r = \mu_r = c_r = \alpha_r = 10^{-5}$, $k_r = 1$, and $\lambda = 0.5$ and a contact angle of 61.4 degrees.

TABLE I
Convergence of the Interface Location

Mesh	L_2 interface error	Ratios
4×4	9.296907e-05	
8×8	2.385825e-05	3.90
16×16	6.045105e-06	3.95
32×32	1.521926e-06	3.97

TABLE II
Convergence of the Pressure Field

Mesh	L_2 pressure error	Ratios
4×4	4.926325e-01	
8×8	1.387477e-01	3.55
16×16	3.812523e-02	3.64
32×32	9.551118e-03	3.99

4.2. Passive Upper Fluid

If the upper fluid is “passive,” the results computed for Marangoni–Bénard convection in a single fluid by Cliffe and Tavener [19] should be recovered. A passive upper fluid was approximated by setting the density, viscosity, expansion, and specific heat ratios to be 10^{-10} . The volume fraction of the lower fluid, where

$$\text{volume fraction} = \frac{v_1}{v_1 + v_2} = \frac{1}{1 + v_r},$$

was varied between 0.1 and 0.99. The width of the domain was set to equal the volume of the lower fluid, i.e., $\lambda = v_1$, so that the aspect ratio of the lower fluid was always equal to one. By setting the conductivity ratio equal to the volume ratio, i.e., $k_r = v_r$, the temperature drop across both fluids was equal for all values of the volume fraction. In the previous computations of convection in a single fluid, the temperature was normalized by the temperature drop across the fluid. The conductivity ratio was adjusted in the above manner in order to make comparisons with the single-fluid calculations easier. Similarly, the length scale in the single-fluid calculations was the depth of the (single) layer, and the critical Marangoni numbers computed for the two-layer case were adjusted appropriately. The critical Marangoni numbers at which symmetry breaking to a one-cell flow (in each fluid) occurs in the two-fluid formulation with a passive upper fluid are shown in Fig. 2. The horizontal dashed line at $Ma = 212.14$ is the corresponding critical value from the one-fluid calculations.

It is perhaps not immediately obvious why the two-fluid calculations with a passive upper fluid approach the corresponding value for a single fluid only in the limit as the depth of the upper fluid approaches zero. The answer lies in the different thermal boundary conditions applied in the two instances. Let subscripts 1 and 2 denote the lower and upper fluids, respectively, and let superscripts 0 and 1 denote, respectively, the trivial conducting solution and a perturbation about the conducting solution. All such perturbations decay for

TABLE III
Convergence of the Velocity Field

Mesh	L_2 velocity error	Ratios
4×4	3.721297e-04	
8×8	3.570628e-05	10.42
16×16	3.301944e-06	10.81
32×32	2.991931e-07	11.04

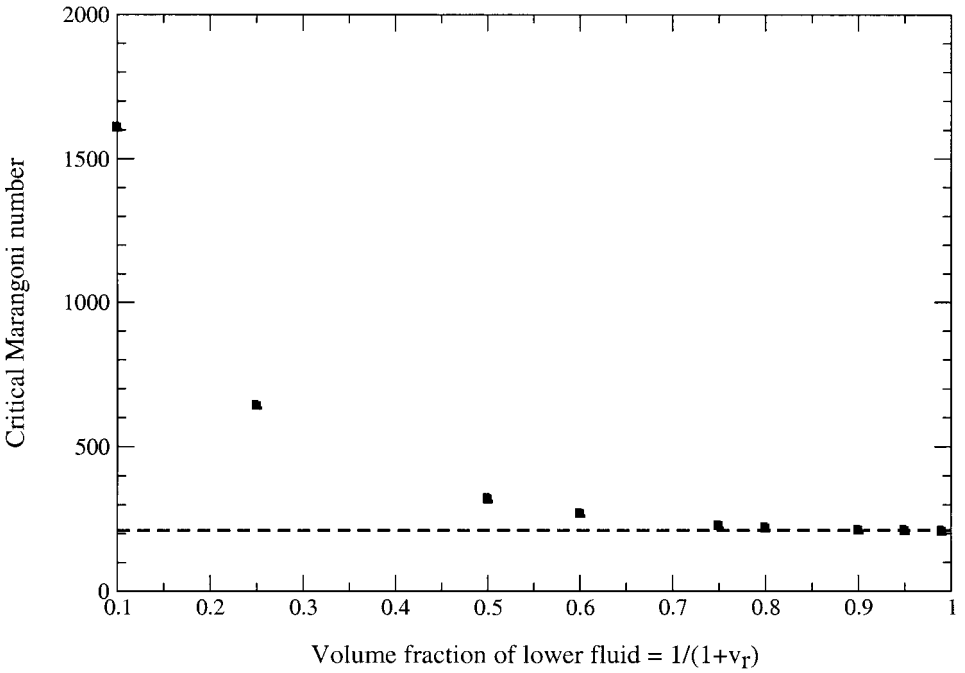


FIG. 2. Critical Marangoni number for the onset of a single-cell flow (in each fluid) as a function of volume fraction of the lower fluid, i.e., $1/(1 + v_r)$, given a passive upper fluid. $Pr = 1$, $Ca = 10^{-5}$, $\rho_r = \mu_r = \alpha_r = c_r = 10^{-10}$, $k_r = v_r$, $\lambda = 1/(1 + v_r)$.

Marangoni numbers less than the critical. Assume that the free surface in the one-fluid case and the interface in the two-fluid case are perpendicular to the y -axis. For a single fluid, the thermal boundary condition at the free surface is

$$\frac{\partial T}{\partial y} = -LT.$$

Here L is the Biot number,

$$L = \frac{hd}{k},$$

where h is the surface thermal conductance, d is the length scale, and k is the thermal conductivity of the fluid. If we perturb about the conducting solution and let

$$T = T^0 + \epsilon T^1,$$

the boundary condition for the linear stability problem is

$$\frac{\partial T^1}{\partial y} = -LT^1. \quad (16)$$

For two immiscible fluids, the thermal boundary condition at their interface is

$$k_1 \frac{\partial T_1}{\partial y} = k_2 \frac{\partial T_2}{\partial y},$$

and if

$$T = T_i^0 + \epsilon T_i^1, \quad i = 1, 2,$$

the leading-order thermal boundary conditions for the linear stability problem are

$$T_1^1 = T_2^1 \tag{17}$$

and

$$k_1 \frac{\partial T_1^1}{\partial y} = k_2 \frac{\partial T_2^1}{\partial y}. \tag{18}$$

If we make the approximation

$$\frac{\partial T_2^1}{\partial y} = -\frac{T_2^1}{d_2}, \tag{19}$$

where d_2 is the depth of the upper fluid, the boundary condition (18) becomes

$$\frac{\partial T_1^1}{\partial y} = \left(\frac{k_2}{k_1 d_2} \right) T_1^1$$

using (17). The two-fluid thermal boundary conditions are equivalent to those for a single fluid (16) if

$$L = \frac{k_2}{k_1 d_2}.$$

However, this equivalence relies on the approximation (19) being appropriate. When d_2 is nonnegligible, (19) can be a very poor approximation, but it becomes increasingly accurate as $d_2 \rightarrow 0$.

4.3. Top Heating for Realistic Parameter Values

When the contact angles are 90 degrees there is a nonconvecting solution of the equilibrium equations in which the temperature profile across the two fluids is piecewise linear, whose gradients are inversely proportional to the thermal conductivities. Odd-cell flows arise at symmetry-breaking bifurcation points at which the Z_2 symmetry about the vertical midplane is broken. Even-cell flows respect this symmetry and arise at transcritical, subspace-breaking bifurcation points. Contact angles other than 90 degrees do not permit nonconvecting solutions, since a temperature gradient must always exist along the interface. Provided the contact angles at both sides are equal, the boundary value problem remains equivariant with respect to a Z_2 symmetry about the vertical midplane and odd-cell flows

TABLE IV
Fluid Properties of Acetonitrile and *n*-Hexane as Reported
by Juel *et al.* [13]

Property	Acetonitrile	<i>n</i> -Hexane
$\rho(10^3 \text{ kg m}^{-3})$	0.776	0.655
$\nu(10^{-6} \text{ m}^2 \text{ s}^{-1})$	0.476	0.458
$k(10^{-1} \text{ J m}^{-1} \text{ s}^{-1} \text{ K}^{-1})$	1.88	1.20
$c_p(10^3 \text{ J kg}^{-1} \text{ K}^{-1})$	2.23	2.27
$\alpha(10^{-3} \text{ K}^{-1})$	1.41	1.41
$\sigma_0(10^{-3} \text{ N m}^{-1})$	28.66	17.89
$\sigma_1(10^{-5} \text{ N m}^{-1} \text{ K}^{-1})$	12.63	10.22

arise at pitchfork bifurcation points. Since there is no longer a conducting solution, there is no invariant subspace from which even-cell flows can arise, and the transcritical bifurcation to even-cell flows is disconnected. Similar features have been discussed by Cliffe and Tavener [19] in the context of single-fluid flows.

In two-fluid convection, the novel possibility exists of instabilities arising despite the fact that the fluid is heated from above, and we will concentrate on this scenario. Juel *et al.* [13] demonstrated experimentally the existence of convection in a perfluorinated oil and silicone oil system that is heated from above. They also presented interesting results from a linear stability analysis of an acetonitrile and *n*-hexane system that is unstable when heated from above (Table IV). We concentrate on the latter system despite the fact that Juel *et al.* [13] do not report experimental results owing to problems of miscibility. Unlike Juel *et al.* [13], we do not assign ΔT^* a positive or negative sign to indicate whether our assigned temperature gradient is parallel or antiparallel to the direction of gravity. Thus all our Marangoni numbers are positive even when the upper boundary is hotter than the lower. The direction of the temperature gradient is determined by the Dirichlet boundary conditions applied to the temperature field at the top and bottom surfaces.

We first show in Fig. 3 a bifurcation diagram for equal amounts of the two fluids and aspect ratio 1.5, for 90-, 89.99-, and 89.89-degree contact angles. The ordinate is the temperature at the midpoint of the interface, i.e., $T(0, h(0))$. When 90-degree contact angles are imposed there exists a conducting solution for all values of the Marangoni number. The temperature at the midpoint of the interface can be calculated analytically for this conducting solution as

$$T_{\text{interface}} = \frac{2k_r}{1 + k_r} = \frac{(2)(0.638)}{1 + 0.638} = 0.779.$$

Notice that the bifurcation from the conducting solution is clearly transcritical. For contact angles other than 90 degrees the bifurcation diagram is disconnected in the expected manner. For contact angles less than 90 degrees, the center of the interface lies further away from the hot top boundary than do the edges and is therefore cooler than the edges, and cooler than the conducting solution. Surface tension gradients will drag fluid from the edges to the middle of the domain, producing downwelling along the centerline of the lower fluid and upwelling along the centerline of the upper fluid. Streamfunction and isotherms for the two types of stable two-cell flows are shown for $Ma = 2100$ and contact angle 89.89 degrees in Figs. 4 and 5.

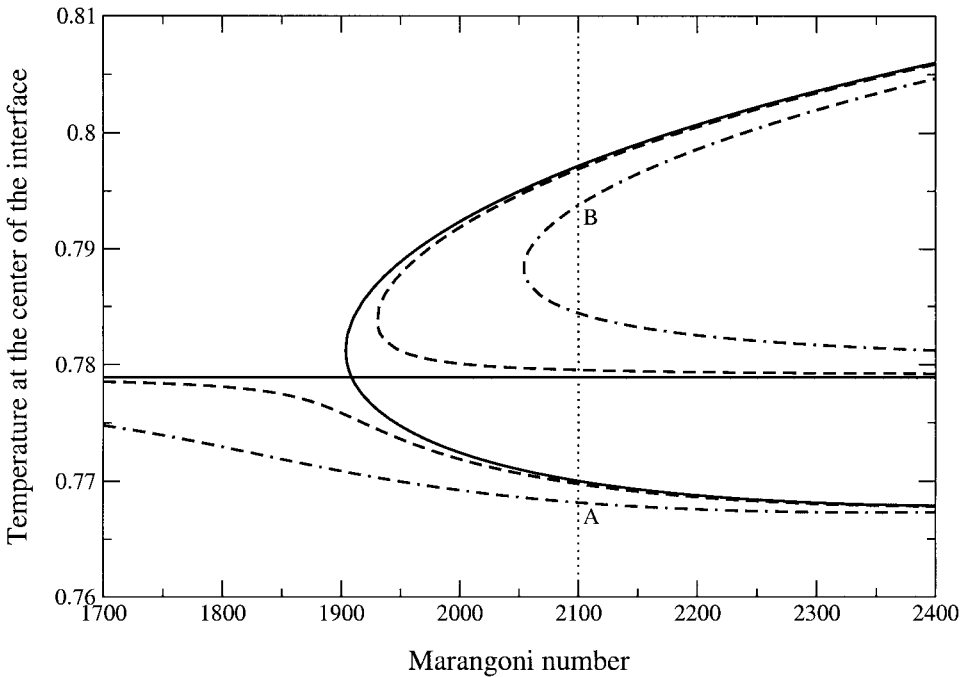


FIG. 3. Bifurcation diagram near instability to two-cell flows when heating from above for contact angles equal to 90 (solid line), 89.99 (dashed line), and 89.89 (chained line) degrees. $Pr = 4.38$, $Ca = 2.5 \times 10^{-6}$, $\rho_r = 0.844$, $\mu_r = 0.812$, $\alpha_r = 1.0$, $c_r = 1.02$, $k_r = 0.638$, $\nu_r = 1.0$, $\lambda = 1.5$.

The physics of heating from above has recently been summarized by Johnson and Narayanan [16]. The simplest instability mechanism, and the only one relevant to the computations reported here, is sketched in Fig. 6. In the upper diagram, a local temperature elevation in the center of the interface is assumed. This lowers the local surface tension and fluid is dragged toward the edges of the domain. It is replaced by hot fluid flowing downward from the top boundary, reinforcing the perturbation. The lower fluid is viscously coupled and there is upwelling of cold fluid from the bottom boundary, which tends to dampen the perturbation. The lower sketch in Fig. 6 shows the opposite scenario. Again, the flow in the upper fluid reinforces the instability, while the flow in the lower fluid tends to reduce it. We now consider the effect of varying the conductivity, volume, density, and specific heat ratios on these mechanisms. For simplicity, we will always consider the case of 90 degree contact angles.

4.3.1. Relative Density and Specific Heat Ratios

The heat carried by the convecting upper fluid depends on the product of its density and its heat capacity. Since the flow in the upper fluid sustains the perturbation, the critical Marangoni number decreases for increasing density ratio and increasing specific heat ratio, as is shown in Figs. 7 and 8, respectively. The effect of the density ratio even in the absence of gravity is at first surprising, but the role of the upper fluid when heating from above has been recognized at least back to the work of Sterling and Scriven [27] and Vidal and Acrivos [28].

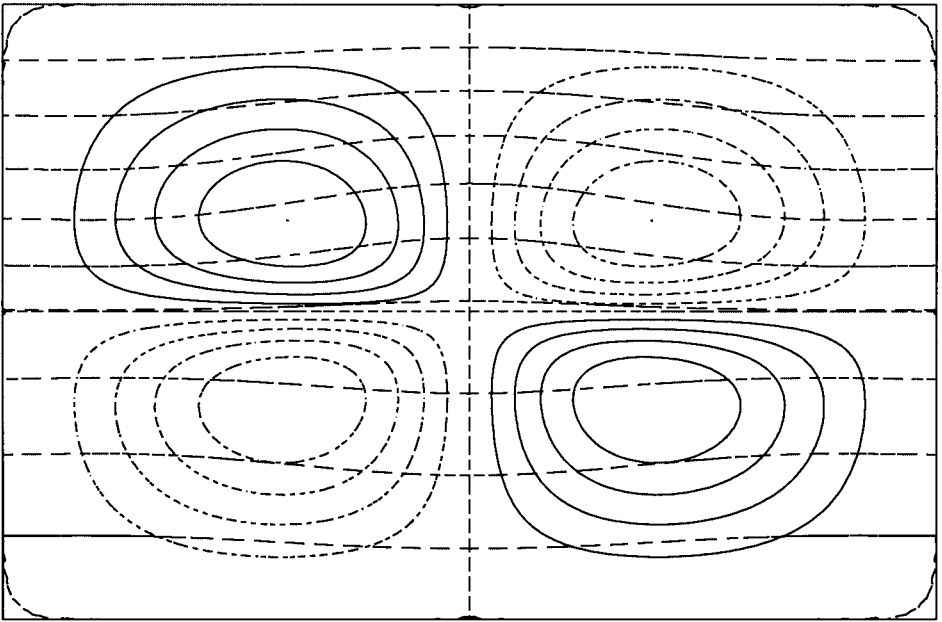


FIG. 4. Streamlines and isotherms when heating from above for the connected two-cell flow at $Ma = 2100$ and contact angle 89.89 degrees (point A, Fig. 3). Solid lines indicate positive values of the streamfunction (anticlockwise circulation) and dashed lines indicate negative values of the streamfunction (clockwise circulation). $Pr = 4.38$, $Ca = 2.5 \times 10^{-6}$, $\rho_r = 0.844$, $\mu_r = 0.812$, $\alpha_r = 1.0$, $c_r = 1.02$, $k_r = 0.638$, $v_r = 1.0$, $\lambda = 1.5$.

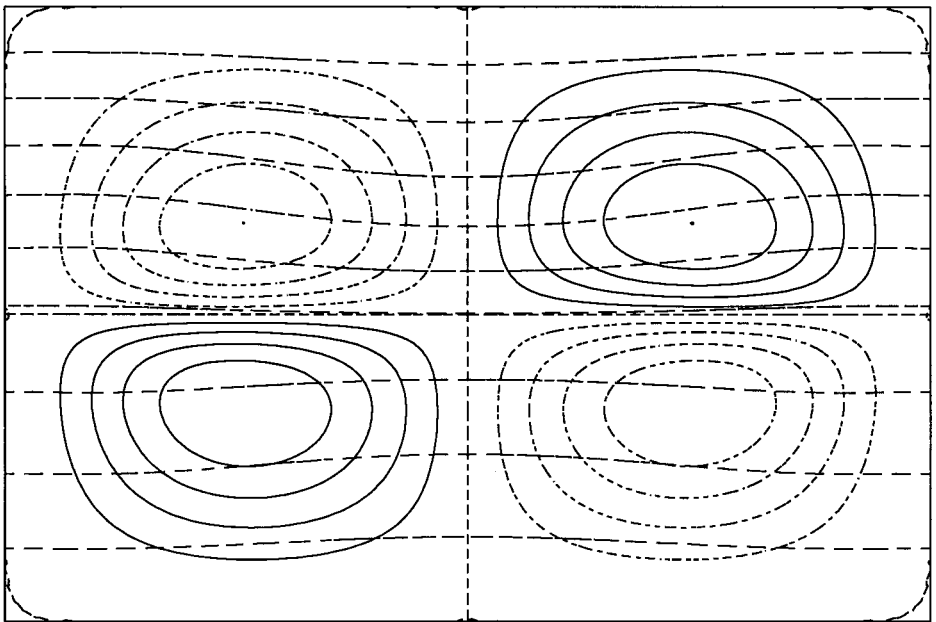


FIG. 5. Streamlines and isotherms when heating from above for the disconnected two-cell flow at $Ma = 2100$ and contact angle 89.89 degrees (point B, Fig. 3). Solid lines indicate positive values of the streamfunction (anticlockwise circulation) and dashed lines indicate negative values of the streamfunction (clockwise circulation). $Pr = 4.38$, $Ca = 2.5 \times 10^{-6}$, $\rho_r = 0.844$, $\mu_r = 0.812$, $\alpha_r = 1.0$, $c_r = 1.02$, $k_r = 0.638$, $v_r = 1.0$, $\lambda = 1.5$.

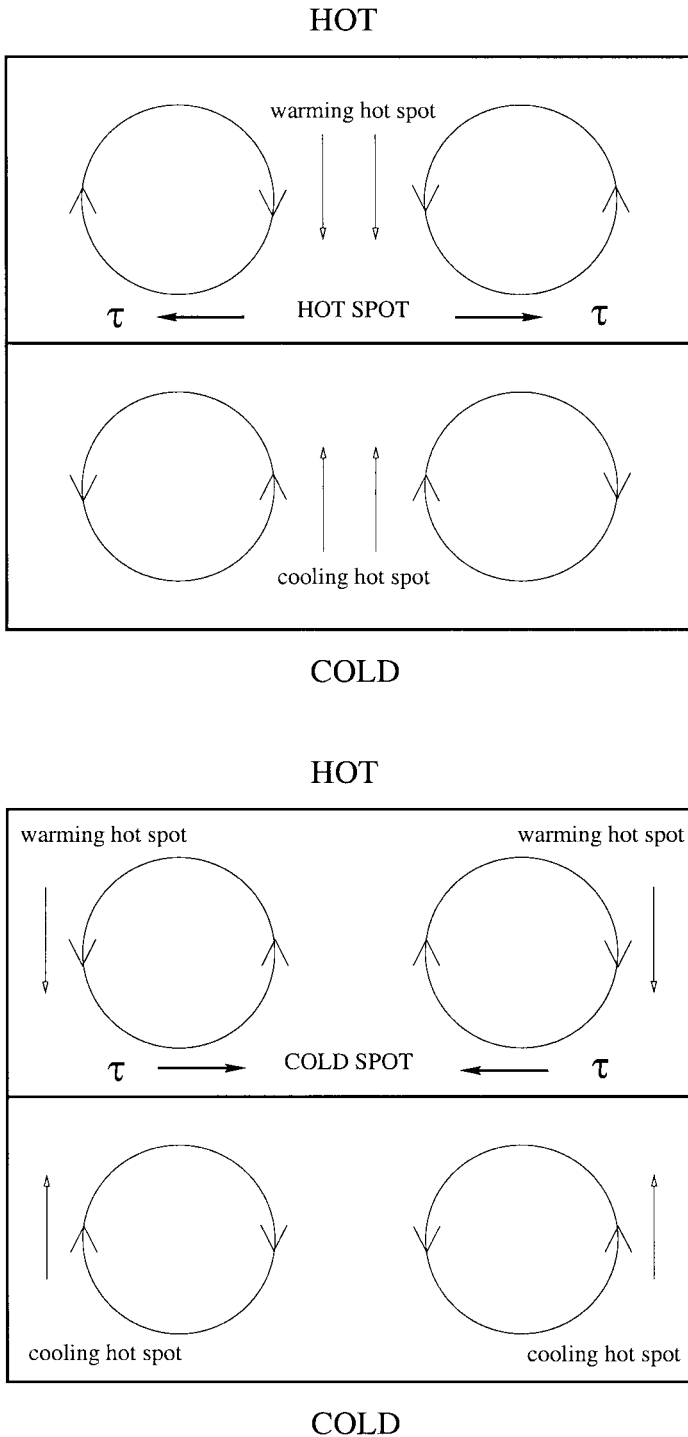


FIG. 6. Thermocapillary instability mechanism when heating from above.

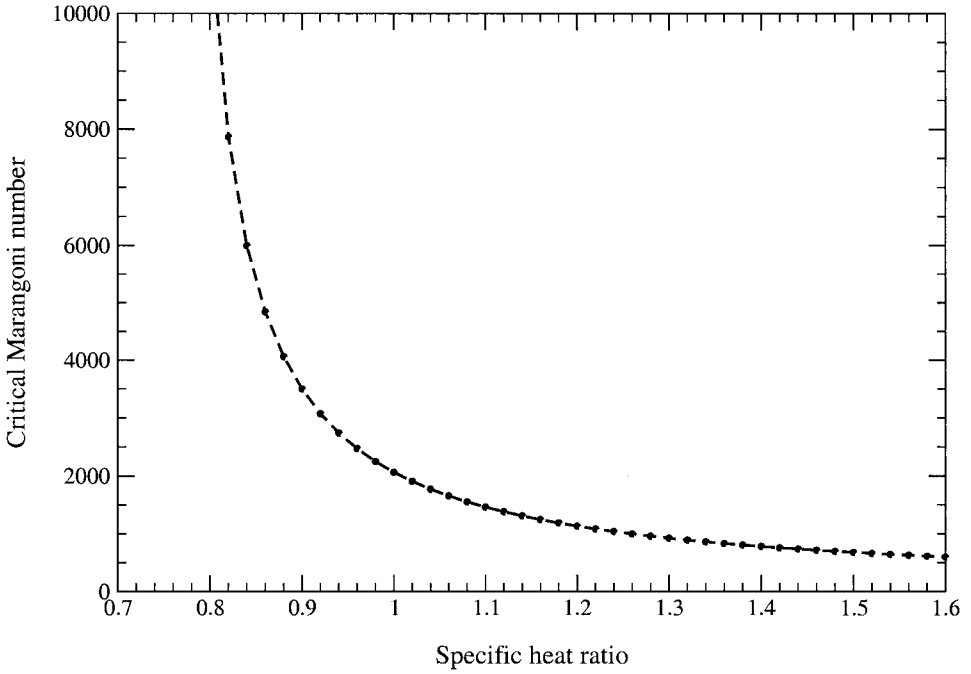


FIG. 7. Effect of specific heat ratio on bifurcation to two-cell flows when heating from above. $Pr = 4.38$, $Ca = 2.5 \times 10^{-6}$, $\rho_r = 0.844$, $\mu_r = 0.812$, $\alpha_r = 1.0$, $k_r = 0.638$, $\nu_r = 1.0$, $\lambda = 1.5$.

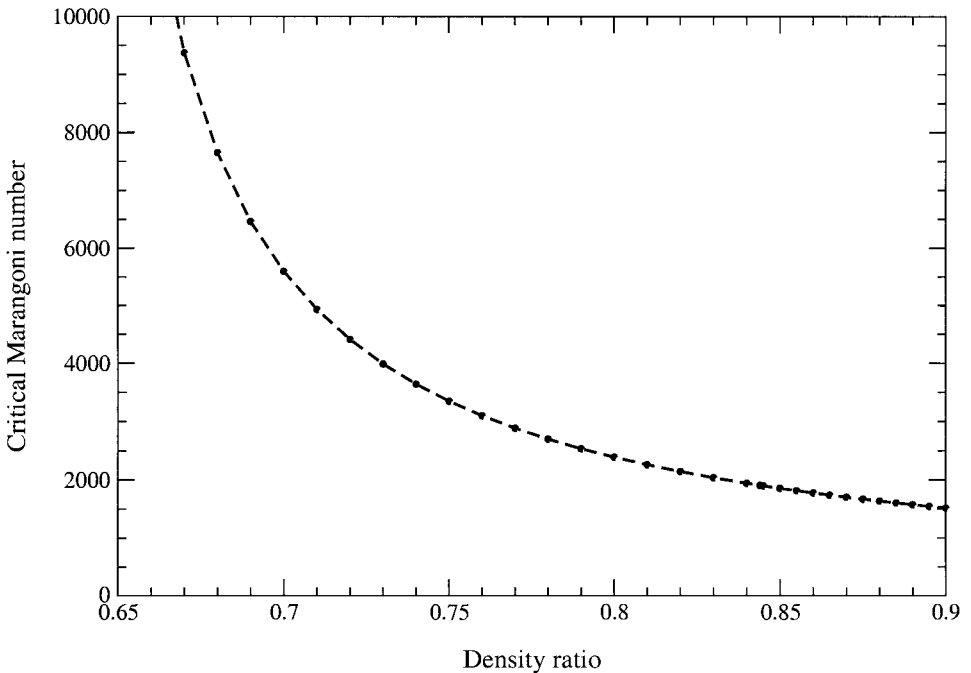


FIG. 8. Effect of density ratio on bifurcation to two-cell flows when heating from above. $Pr = 4.38$, $Ca = 2.5 \times 10^{-6}$, $\mu_r = 0.812$, $\alpha_r = 1.0$, $c_r = 1.02$, $k_r = 0.638$, $\nu_r = 1.0$, $\lambda = 1.5$.

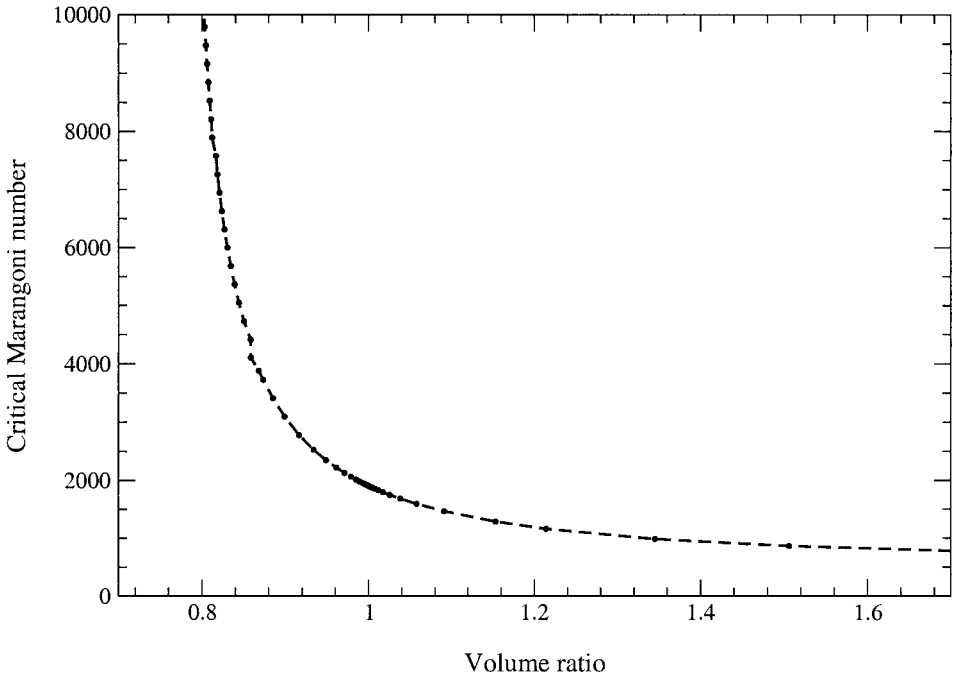


FIG. 9. Effect of volume ratio on bifurcation to two-cell flows when heating from above. $Pr = 4.38$, $Ca = 2.5 \times 10^{-6}$, $\rho_r = 0.844$, $\mu_r = 0.812$, $\alpha_r = 1.0$, $c_r = 1.02$, $k_r = 0.638$, $\lambda = 1.5$.

4.3.2. Volume Ratio

For the conducting solution, the temperature at the interface is given by

$$T_{\text{interface}} = \frac{2k_r}{v_r + k_r}.$$

For a fixed conductivity ratio, the temperature at the interface increases as the volume ratio decreases, approaching the temperature of the upper boundary. The driving force for the instability decreases and so the critical Marangoni number increases, as shown in Fig. 9.

4.3.3. Conductivity Ratio

The temperature at the interface of the conducting solution can also be written as

$$T_{\text{interface}} = \frac{2}{1 + v_r/k_r}.$$

As the conductivity ratio increases at fixed volume ratio, the temperature at the interface increases, more closely approaching that of the upper boundary. The driving force for the instability decreases and the critical Marangoni number increases, as shown in Fig. 10.

4.3.4. The Effect of Gravity

The effect of buoyancy on the critical Marangoni number is shown in Fig. 11. We note that even when stabilizing buoyancy effects are present, instability on heating from above

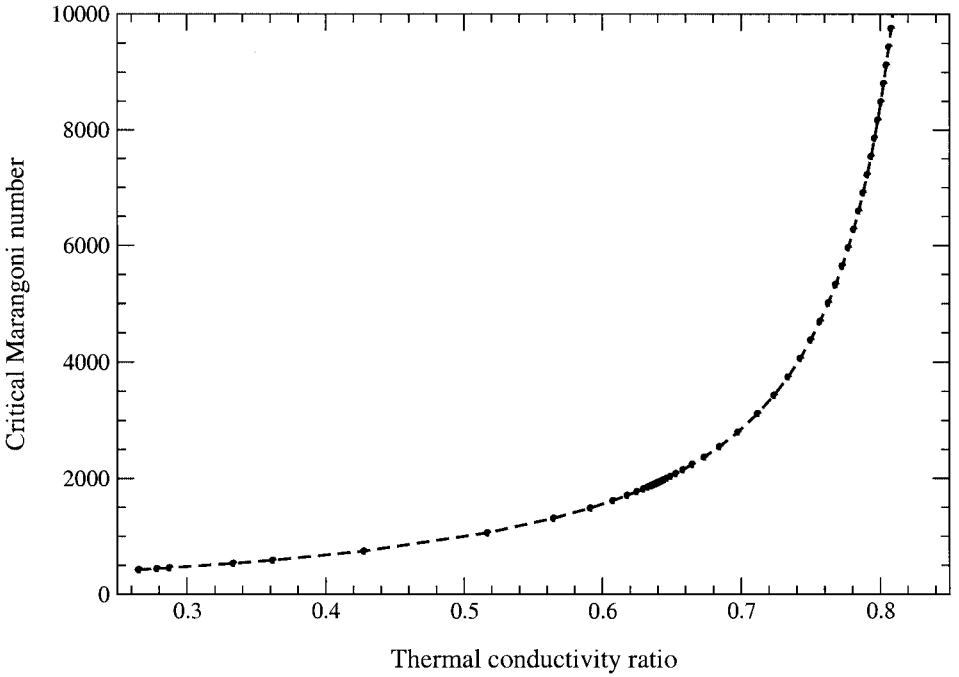


FIG. 10. Effect of conductivity ratio on bifurcation to two-cell flows when heating from above. $Pr = 4.38$, $Ca = 2.5 \times 10^{-6}$, $\rho_r = 0.844$, $\mu_r = 0.812$, $\alpha_r = 1.0$, $c_r = 1.02$, $\nu_r = 1.0$, $\lambda = 1.5$.

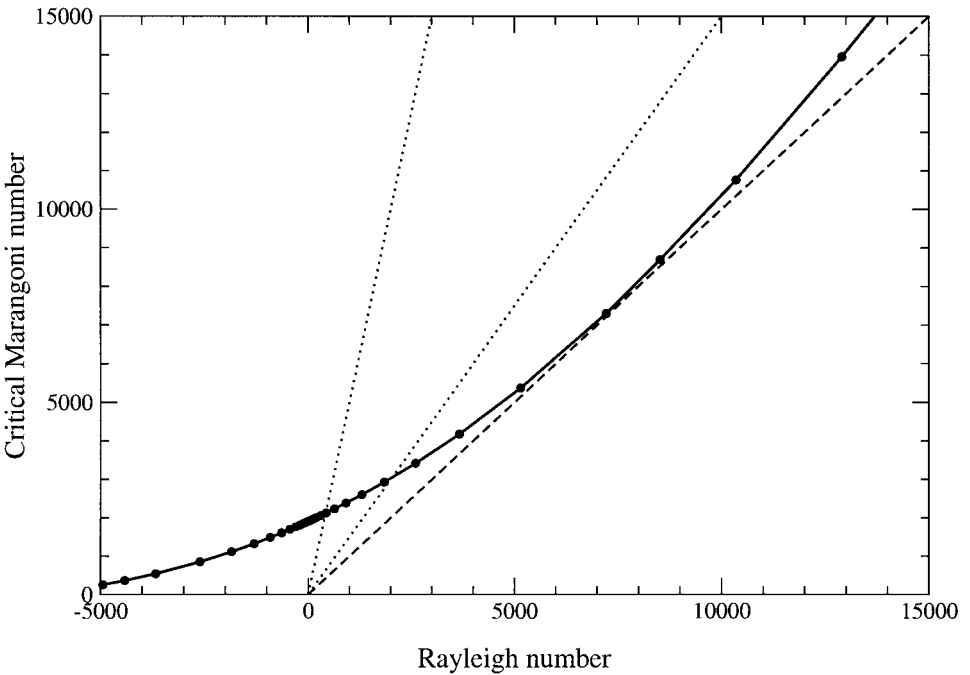


FIG. 11. Effect of buoyancy on bifurcation to two-cell flows when heating from above. The dashed line through the origin has slope 1 and is approximately tangential to the locus of critical points. The dotted lines through the origin have slopes 5 and 1.5. For the fluids considered by Juel *et al.* [13], the two dotted lines correspond to overall fluid depths of 1.5 and 3 mm and the dashed line to an overall fluid depth of approximately 3.5 mm. $Pr = 4.38$, $Ca = 2.5 \times 10^{-6}$, $G = 5 \times 10^4$, $\rho_r = 0.844$, $\mu_r = 0.812$, $\alpha_r = 1.0$, $c_r = 1.02$, $k_r = 0.638$, $\nu_r = 1.0$, $\lambda = 1.5$.

can still occur. The Galileo number was set to be 5×10^4 and the other parameters were as before. In particular, the volume ratio was fixed and equal to one.

As has been reemphasized recently by Regnier *et al.* [29] and Velarde *et al.* [4], it is important to ensure that the Boussinesq approximation is appropriate. In order for the Boussinesq approximation to be valid for two-fluid convection, the product $\alpha_i \Delta T_i^*$ must be small in each liquid, where ΔT_i^* is the temperature difference across the individual liquid. (For the flows considered here, an almost equivalent requirement is that the ratio Ra/G be small.) Further, for the linear relationship between surface tension and temperature to be valid, the ratio $\sigma_1 \Delta T^* / \sigma_0$ must remain small. When the temperature difference between the two plates is on the order of a single degree, $\alpha_i \Delta T_i^* < 10^{-3}$ in both liquids and $\sigma_1 \Delta T^* / \sigma_0 < 10^{-2}$, and the use of the Boussinesq approximation is justified.

For the two fluids considered here

$$Ra = 2.67 \times 10^{11} d^3 \Delta T^* \quad \text{and} \quad Ma = 3.15 \times 10^6 d \Delta T^*.$$

In Fig. 12, we plot the ratio of Marangoni number to Rayleigh number as a function of depth d for any given ΔT^* . Clearly as d increases, the Rayleigh number dominates the Marangoni number. In Fig. 11, we observe that a line of slope 1 passing through the origin is approximately tangential to the locus of critical points. Accordingly, if the depth is sufficiently large that the Marangoni number is less than the Rayleigh number, the conducting solution will be stable. From Fig. 12, we see that this occurs when the overall depth exceeds approximately 3.5 mm. For overall depths greater than 3.5 mm we therefore expect the stabilizing effects of gravity to dominate the destabilizing effects of surface tension.

Juel *et al.* [13, Figs. 5 and 6] report the result of a linear stability analysis performed in a laterally unbounded domain for both top heating and bottom heating, for overall depths

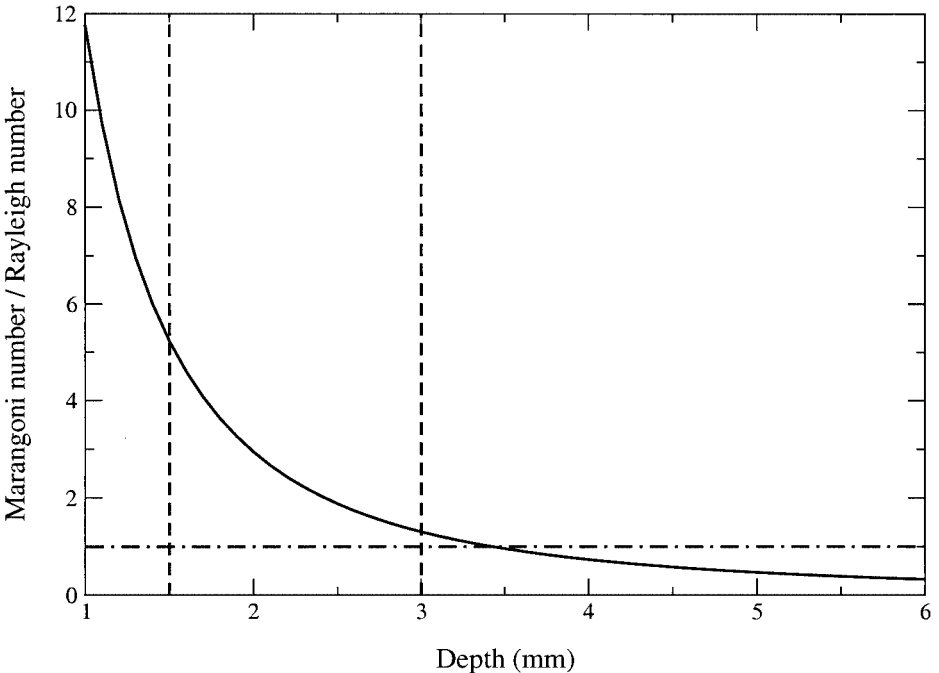


FIG. 12. Ratio of Marangoni number to Rayleigh number as a function of depth.

of 1.5, 3.0, 4.5, and 6.0 mm. At a volume ratio of 1 ($d_1/d_{\text{tot}}=0.5$), the latter two cases should be stable. From Fig. 12, the ratio of the Marangoni to Rayleigh numbers at overall depths of 1.5 and 3 mm are approximately 5 and 1.5, respectively. At these particular ratios the critical Marangoni numbers from Fig. 11 are 2000 and 3000, respectively. These values correspond to temperature difference of 0.4 and 0.3 degrees, respectively, in reasonable agreement with those reported by [13], and well within the range for which the Boussinesq approximation is valid. Further, we conjecture that the discontinuous change in the slope of the critical temperature difference as a function of volume fraction and the discontinuous change in the critical wavenumber as a function of volume fraction, reported in [13, Figs. 5 and 6], are manifestations of the observation described above.

5. CONCLUSIONS

We have formulated the two-fluid Rayleigh–Marangoni–Bénard convection problem with a deformable interface, invoking the usual Boussinesq approximation. A Landau transformation from the physical domain to a reference domain was used to determine the location of the interface. The combined system of mapping, continuity, momentum, and energy equations was solved in weak form in two dimensions using the finite-element method. Numerical bifurcation techniques were used to compute surface-tension and buoyancy-driven instabilities in finite aspect-ratio domains. The role of changing volume fraction, of particular interest to the crystal-growing industry, can be investigated efficiently using the approach described here. We have concentrated on the interesting case of heating from above using real fluid properties. Our results are consistent with physical arguments and agree well quantitatively with those of other authors who have used traditional linear stability approaches on unbounded domains. A two-dimensional finite-element approach has the considerable advantages of allowing domains of finite lateral extent to be studied, the effect of contact angles other than 90 degrees to be quantified, the nonlinear development of flows to be examined, and the stability of convecting solutions to be determined.

APPENDIX: WEAK FORMULATION

For ease of reading, we drop the $*$ notation indicating dimensional quantities in the following discussion. All quantities, such as velocities and pressures, are assumed to be dimensional. The final weak form is then nondimensionalized to produce Eqs. (8) and (9).

A weak form of the steady momentum equations is

$$\begin{aligned} & \int_{\Omega_1} \{(\bar{\rho}_1(\mathbf{u} \cdot \nabla)\mathbf{u} + \rho_1 g \mathbf{j}) \cdot \mathbf{w} + \tau_1 : \nabla \mathbf{w}\} dA - \int_{\Gamma_i} \tau_1 \mathbf{n}_1 \cdot \mathbf{w} ds \\ & + \int_{\Omega_2} \{(\bar{\rho}_2(\mathbf{u} \cdot \nabla)\mathbf{u} + \rho_2 g \mathbf{j}) \cdot \mathbf{w} + \tau_2 : \nabla \mathbf{w}\} dA - \int_{\Gamma_i} \tau_2 \mathbf{n}_2 \cdot \mathbf{w} ds = 0. \end{aligned}$$

Combining the two boundary integral terms above we have

$$\begin{aligned} & \int_{\Omega_1} \{(\bar{\rho}_1(\mathbf{u} \cdot \nabla)\mathbf{u} + \rho_1 g \mathbf{j}) \cdot \mathbf{w} + \tau_1 : \nabla \mathbf{w}\} dA \\ & + \int_{\Omega_2} \{(\bar{\rho}_2(\mathbf{u} \cdot \nabla)\mathbf{u} + \rho_2 g \mathbf{j}) \cdot \mathbf{w} + \tau_2 : \nabla \mathbf{w}\} dA + \int_{\Gamma_i} [\tau \mathbf{n}] \cdot \mathbf{w} ds = 0, \end{aligned}$$

where $[\cdot]$ denotes the jump across the interface and $\mathbf{n} = \mathbf{n}_1 = -\mathbf{n}_2$ on the interface points from Ω_1 into Ω_2 . Applying the dynamic boundary condition at the interface (5),

$$\int_{\Omega_1} \{(\bar{\rho}_1(\mathbf{u} \cdot \nabla)\mathbf{u} + \rho_1 g \mathbf{j}) \cdot \mathbf{w} + \tau_1 : \nabla \mathbf{w}\} dA + \int_{\Omega_2} \{(\bar{\rho}_2(\mathbf{u} \cdot \nabla)\mathbf{u} + \rho_2 g \mathbf{j}) \cdot \mathbf{w} + \tau_2 : \nabla \mathbf{w}\} dA - \int_{\Gamma_i} (K \sigma \mathbf{n} + (\mathbf{t} \cdot \nabla \sigma) \mathbf{t}) \cdot \mathbf{w} ds = 0.$$

Using

$$\frac{d\mathbf{t}}{ds} = K\mathbf{n},$$

we have

$$\int_{\Omega_1} \{(\bar{\rho}_1(\mathbf{u} \cdot \nabla)\mathbf{u} + \rho_1 g \mathbf{j}) \cdot \mathbf{w} + \tau_1 : \nabla \mathbf{w}\} dA + \int_{\Omega_2} \{(\bar{\rho}_2(\mathbf{u} \cdot \nabla)\mathbf{u} + \rho_2 g \mathbf{j}) \cdot \mathbf{w} + \tau_2 : \nabla \mathbf{w}\} dA - \int_{\Gamma_i} \left(\sigma \frac{d\mathbf{t}}{ds} + (\mathbf{t} \cdot \nabla \sigma) \mathbf{t} \right) \cdot \mathbf{w} ds = 0,$$

or

$$\int_{\Omega_1} \{(\bar{\rho}_1(\mathbf{u} \cdot \nabla)\mathbf{u} + \rho_1 g \mathbf{j}) \cdot \mathbf{w} + \tau_1 : \nabla \mathbf{w}\} dA + \int_{\Omega_2} \{(\bar{\rho}_2(\mathbf{u} \cdot \nabla)\mathbf{u} + \rho_2 g \mathbf{j}) \cdot \mathbf{w} + \tau_2 : \nabla \mathbf{w}\} dA - \int_{\Gamma_i} \frac{d(\sigma \mathbf{t})}{ds} \cdot \mathbf{w} ds = 0,$$

and finally

$$\int_{\Omega_1} \{(\bar{\rho}_1(\mathbf{u} \cdot \nabla)\mathbf{u} + \rho_1 g \mathbf{j}) \cdot \mathbf{w} + \tau_1 : \nabla \mathbf{w}\} dA + \int_{\Omega_2} \{(\bar{\rho}_2(\mathbf{u} \cdot \nabla)\mathbf{u} + \rho_2 g \mathbf{j}) \cdot \mathbf{w} + \tau_2 : \nabla \mathbf{w}\} dA + \int_{\Gamma_i} \sigma \mathbf{t} \cdot \frac{d\mathbf{w}}{ds} ds = 0,$$

on integrating the surface integral by parts.

A weak form of the steady energy (temperature) equations is

$$\int_{\Omega_1} (\bar{\rho}_1 c_1(\mathbf{u} \cdot \nabla T) \xi + k_1(\nabla T \cdot \nabla \xi)) dA - \int_{\Gamma_i} k_1((\nabla T)_1 \cdot \mathbf{n}_1) \xi ds + \int_{\Omega_2} (\bar{\rho}_2 c_2(\mathbf{u} \cdot \nabla T) \xi + k_2(\nabla T \cdot \nabla \xi)) dA - \int_{\Gamma_i} k_2((\nabla T)_2 \cdot \mathbf{n}_2) \xi ds = 0.$$

Combining the two boundary integral terms above we have

$$\int_{\Omega_1} (\bar{\rho}_1 c_1(\mathbf{u} \cdot \nabla T) \xi + k_1(\nabla T \cdot \nabla \xi)) dA + \int_{\Omega_2} (\bar{\rho}_2 c_2(\mathbf{u} \cdot \nabla T) \xi + k_2(\nabla T \cdot \nabla \xi)) dA + \int_{\Gamma_i} [k(\nabla T \cdot \mathbf{n})] \xi ds = 0,$$

where $[\cdot]$ denotes the jump across the interface and $\mathbf{n} = \mathbf{n}_1 = -\mathbf{n}_2$ on the interface points

from Ω_1 into Ω_2 . By continuity of thermal flux, (6),

$$\int_{\Omega_1} (\bar{\rho}_1 c_1 (\mathbf{u} \cdot \nabla T) \xi + k_1 (\nabla T \cdot \nabla \xi)) dA + \int_{\Omega_2} (\bar{\rho}_2 c_2 (\mathbf{u} \cdot \nabla T) \xi + k_2 (\nabla T \cdot \nabla \xi)) dA = 0.$$

ACKNOWLEDGMENTS

The authors thank Dr. Anne Juel for her critical reading of the manuscript and Professor Robert Kelly for his helpful comments.

REFERENCES

1. M. J. Block, Surface tension as the cause of Bénard cells and surface deformation in a liquid film, *Nature*, **178**, 650 (1956).
2. J. R. A. Pearson, On convection cells induced by surface tension, *J. Fluid Mech.* **4**, 489 (1958).
3. D. A. Nield, Surface tension and buoyancy effects in cellular convection, *J. Fluid Mech.* **19**, 341 (1964).
4. M. G. Velarde, A. A. Nepomnyashchy, and M. Hennenberg, Onset of oscillatory interfacial instabilities and wave motions in Bénard layers, *Adv. Appl. Mech.* **37**, 167 (2001).
5. C. D. Andereck, P. W. Colovas, M. M. Degen, and Y. Y. Renardy, Instabilities in two layer Rayleigh-Bénard convection: Overview and outlook, *Int. J. Eng. Sci.* **36**, 1451 (1998).
6. R. W. Zeren and W. C. Reynolds, Thermal instabilities in two-fluid horizontal layers, *J. Fluid Mech.* **53**, 305 (1972).
7. N. Imaishi and K. Fujinawa, Theoretical study of the stability of two-fluid layers, *J. Chem. Eng. Jpn.* **7**, 81 (1974).
8. N. Imaishi and K. Fujinawa, Thermal instability in two-fluid layers, *J. Chem. Eng. Jpn.* **7**, 87 (1974).
9. S. Rasenat, F. H. Busse, and I. Rehberg, A theoretical and experimental study of double-layer convection, *J. Fluid Mech.* **199**, 519 (1989).
10. Y. Y. Renardy and D. D. Joseph, Oscillatory instability in a Bénard problem of two fluids, *Phys. Fluids* **28**, 788 (1985).
11. Y. Y. Renardy and M. Renardy, Perturbation analysis of steady and oscillatory onset in a Bénard problem of two fluids, *Phys. Fluids* **28**, 2699 (1985).
12. Y. Y. Renardy and M. Renardy, Bifurcating solutions at the onset of convection in the Bénard problem of two fluids, *Physica D*, **32**, 227 (1988).
13. A. Juel, J. M. Burgess, W. D. McCormick, J. B. Swift, and H. L. Swinney, Surface tension-driven convection patterns in two liquid layers, *Physica D* **143**, 169 (2000).
14. Ph. Géoris, M. Hennenberg, I. B. Simanovskii, A. Nepomniashchy, and I. Wertgeim, Thermocapillary convection in a multilayer, *Phys. Fluids A* **5**, 1575 (1993).
15. Ph. Géoris, M. Hennenberg, G. Lebon, and J. C. Legros, Investigation of thermocapillary convection in a three-liquid-layer system, *J. Fluid Mech.* **389**, 209 (1999).
16. D. Johnson and R. Narayanan, Marangoni convection in multiple bounded fluid layers and its application to materials processing, *Philos. Trans.* **356**, 885 (1998).
17. D. Johnson and R. Narayanan, A tutorial on the Rayleigh-Marangoni-Bénard problem with multiple layers and side-wall effects, *Chaos* **9**, 124 (1999).
18. H. C. Nataf, S. Moreno, and P. Cardin, What is responsible for thermal coupling in layered convection?, *J. Phys. France* **49**, 1707 (1988).
19. K. A. Cliffe and S. J. Tavener, Marangoni-Bénard convection with a deformable free surface, *J. Comput. Phys.* **145**, 193 (1998).
20. K. A. Cliffe, T. J. Garratt, and A. Spence, Eigenvalues of the discretized Navier-Stokes equations with application to the detection of Hopf bifurcations, *Adv. Comp. Math.* **1**, 337 (1993).
21. S. J. Tavener, Stability of the O(2)-symmetric flow past a sphere in a pipe, *Phys Fluids A* **6**, 3884 (1994).

22. A. Griewank and G. Reddien, The calculation of Hopf points by a direct method, *IMA J. Numer. Anal.* **3**, 295 (1983).
23. K. A. Cliffe and S. J. Tavener, Implementation of extended systems using symbolic algebra, in *Continuation Methods in Fluid Dynamics, Notes on Numerical Fluid Mechanics*, edited by D. Henry and A. Bergeon (Vieweg, Braunschweig/Wiesbaden, 2000), p. 81.
24. B. Werner and A. Spence, The computation of symmetry-breaking bifurcation points, *SIAM J. Numer. Anal.* **21**, 388 (1984).
25. B. Werner, Regular systems for bifurcation points with underlying symmetries, in *Numerical Methods for Bifurcation Problems*, edited by T. Küpper, H. D. Mittelman, and H. Weber (Birkhäuser, Basel, 1984), Vol. 70, p. 562.
26. B. Werner, Eigenvalue problems with the symmetry of a group and bifurcations, in *Continuation and Bifurcations: Numerical Techniques and Applications*, edited by D. Roose, B. Dedier, and A. Spence (Kluwer, Dordrecht, 1990), p. 71.
27. C. V. Sternling and L. E. Scriven, Interfacial turbulence: Hydrodynamic instability and the Marangoni effect, *AICh J.* **5**, 514 (1959).
28. A. Vidal and A. Acrivos, Nature of the neutral state in surface tension driven convection, *Phys. Fluids* **9**, 615 (1966).
29. V. C. Regnier, P. C. Dauby, and G. Lebon, Linear and nonlinear Rayleigh-Bénard-Marangoni instability with surface deformations, *Phys. Fluids* **12**, 2787 (2000).